Hydrophobic double walled carbon nanotubes interaction with phopholipidic model membranes: 1H-, 2H-, 31P NMR and ESR study

Jean-Claude Debouzy, David Crouzier, Emmanuel Flahaut

Hydrophobic double walled carbon nanotubes interaction with phopholipidic model membranes: ^{1}H-, ^{2}H-, ^{31}P NMR and ESR study

J.C. Debouzy[a], D. Crouzier[a,*], E. Flahaut[b,c]

[a] CRSSA, Département de Radiobiologie et de Biophysique, 24, Avenue des Maquis du Grésivaudan, 38702 La Tronche Cedex, France
[b] Université de Toulouse, UPS, INP, Institut Carnot Cirimat, 118, Route de Narbonne, F-31062 Toulouse Cedex 9, France
[c] CNRS, Institut Carnot Cirimat, F-31062 Toulouse, France

A B S T R A C T

The interactions of carbon nanotubes synthesized by catalytic chemical vapour deposition with phospholipidic bilayers, mimicking biological membranes, have been investigated using solid state ^{31}P- and ^{2}H NMR, ^{1}H- and ^{31}P NMR in liquids and ESR studies. It was found that carbon nanotubes can integrate the bilayer, depending on the overall cohesion of the membrane used. Whereas no direct interaction can be observed in small unilamellar vesicles or directly in the presence of short-chained phospholipids, carbon nanotubes incorporate into the membrane of multibilayers. The result is a significant 2–3 K lowering of the transition temperature in multibilayers of dimyristoyl lecithins, which is more markedly associated with increased fluidity in the most superficial part of the membrane below the transition temperature (292–300 K range). However, no ionophoric property was found on large unilamellar vesicles.

Keywords:
Carbon nanotubes
Membranes
ESR
NMR

1. Introduction

Carbon nanotubes (CNTs) that belong to the class of nanoparticles, consist of carbon atoms arranged in hexagonal sp^2 structures, themselves organized in tubular superstructures (part of the family of fullerenes, besides other allotropic forms of carbon, such as diamond and graphite). Following the preparation method, the dimensions and number of CNT walls dramatically differ, from single-wall systems (diameters ranging from 0.4 to 2 nm with a length of several μm), while multi-walled CNTs range from 2 to 50 nm (up to 100 nm) in diameter for 1–50 μm in length (Lin et al., 2004). This important diversity directly results from the synthesis method used: catalytic chemical vapour deposition (Cassell et al., 1999; Flahaut et al., 2003), electric arc discharge (Journet et al., 1997), or laser ablation (Bronikowski et al., 2001), as well as high pressure carbon monoxide (Thess et al., 1996) and surface mediated growth of vertically aligned tubes. Each method produces CNTs of different quality, mainly differing by the chemical purity, the presence of residual catalyst and the presence of other forms of carbon species, such as amorphous or graphitic. Finally, specific physico-chemical, mechanical, thermal or electrical properties can be obtained and various applications are currently available, not only in industrial (construction, car assembly, chemistry, surface treatments, and thermal isolation) and domestic uses, in foodstuffs, sun creams, and fabrics (Stern and McNeil, 2008). More recently, biomedical and therapeutic applications have been proposed (Ning et al., 2007). However, a prerequisite for any medical use is the absence of any toxicity, which depends on the degree of systemic bioavailability of such compounds. Interestingly, the evidence for asbestos related occupational disease pointed out the link between toxicity and nanostructures. In the case of CNTs, interactions with biological systems were almost unknown up to the end of the 20th century and remained to be studied and understood. The study of such interactions rests currently with two basic properties of carbon nanotubes. First, their small size and high specific surface area, as well as secondly, possible defects or free carbon residues in these structures which potentially confer functional ability to penetrate living organisms by crossing lipid barriers, possibly leading to irreversible cell damage perhaps by inflammation and/or oxidative stress (Englert, 2004). Besides, most of the CNT preparation methods use heavy metals such as Ni, Co, Mo and Fe as catalysts, which also exert specific toxic effects. As part of the possible biological or medical uses of CNTs, for instance as drug (Mehra et al., 2008), DNA (Lee and Mijovic, 2009) or MRI contrast agent (Faraj et al., 2008) carriers, harmful effects should be studied and cytotoxicity assessed. Alongside different studies performed on lungs after respiratory exposure to CNTs including inflammation, granuloma formation or ROS related damages (Donaldson et al., 2006), various cell studies (e.g. keratinocytes (Monteiro-Riviere et al., 2005), fibroblasts (Tian et al., 2006), and embryo kidney cells (Cui et al., 2005)) have addressed more or less specific mechanisms including membrane permeation for hydrosoluble derivatives, inflammation, cell

* Corresponding author. Fax: +33 4 76 63 69 22.
E-mail address: david.crouzier@wanadoo.fr (D. Crouzier).

doi:10.1016/j.etap.2010.05.002

apoptosis or immune perturbations (Monteiro-Riviere et al., 2005). Conversely other studies found neither alteration in cell viability or metabolism in human umbilical vein endothelial cells (Flahaut et al., 2006). By way of contrast there are only few reports of more general aspecific interactions of CNTs with membranes (Artyukhin et al., 2005; Thauvin et al., 2008; Wallace and Sansom, 2009). This paper presents such a study, using double wall nanotubes (DWNTs) as CNTs and various phospholipidic membrane models to mimic unfunctionalised membranes, which employs NMR and ESR methods.

2. Materials and methods

2.1. Synthesis and characterisation of CNTs

DWNTs were produced by CCVD decomposition of CH_4 over $Mg_{1-x}Co_xO$ solid solution containing small addition of molybdenum. After the CCVD, the catalyst and by products were removed by treatment of the sample with a concentrated aqueous HCl solution. High-resolution transmission electron microscopy showed that a typical sample consists of *ca.* 80% DWNTs, 20% Single walled nanotubes, and a few triple-walled carbon nanotubes. The diameter distribution of the DWNTs ranged from 0.5 to 2.5 nm for inner tubes and from 1.2 to 3.2 nm for outer tubes. The length of individual DWNTs usually ranges between 1 and 10 μm, although bundles may be much longer (up to 100 μm at least). Due to the synthesis and catalyst-elimination process, the walls of the DWNTs are not expected to be functionalized and certainly not by oxygen-containing functional groups.

2.2. Membranes preparation

L-α-Phosphatidyl choline (EPC) and phosphatidic acid (EPA) from egg yolk and synthetic dimyristoyl phosphatidyl choline (DMPC) were obtained from Sigma, la Verpillère, France. DMPC deuterated on both chains (DMPD-d_{54}) was purchased from Interchim, Montluçon, France.

2.2.1. Small unilamellar vesicles (SUV)

EPC in its chloroformic solution (100 mg/ml) was evaporated to a film and resuspended in pure D_2O to a final lipid concentration of 10 mM in 500 μl. SUV were formed by 1 h bath sonication. For CNTs (0.2 mg)/SUV systems, CNTs was either externally added to the vesicles or mixed to the chloroformic EPC solution before evaporation and sonication.

2.2.2. Large unilamellar vesicles (LUV)

LUV were prepared following the method of Szoka and Papahadjopoulos. Briefly, EPC and EPA were mixed in their chloroformic solution (respectively 100 and 10 mg/ml, 9/1: M/M); the solvent was removed by an evaporation under reduced pressure, followed by freeze drying. The pellet was then suspended in 5 ml ether-internal medium (NaH_2PO_4, pH6.5, 0.4 M), 1/4 (v/v) then sonicated twice (2× 2 min). The phase reversion was obtained by slow evaporation under low pressure (N_2 atmosphere). The external medium was then added (NaH_2PO_4, pH6.5, 0.4 M), and polycarbonate filters with decreasing porosities were finally used to calibrate the vesicles to a final diameter of 0.4 μm and a total lipid concentration of 20 mM.

2.2.3. Multilayers vesicles (MLV)

DMPC in its chloroformic solution was evaporated to a film and resuspended in pure D_2O. The liposomes were formed by fast freezing and thawing cycles. The final lipid concentration was 50 mM and CNS/lipid ratio was 1:25 W/M. For ^{2}H NMR experiments, lyophilized DMPC containing 20% phospholipids perdeuterated chains (DMPC-d_{54}) were used and MLV formed in deuterium-depleted water.

2.3. NMR experiments

2.3.1. High-resolution NMR

^{1}H NMR experiments were recorded at 300 K on a Bruker AM-400 spectrometer using a 4000 Hz spectral width, 32 K digitization points, a recycling delay of 2 s and a presaturation of the solvent resonance was used for all the experiments in aqueous medium.

^{13}P NMR experiments in LUV were recorded at 300 K on a Bruker AM-400 spectrometer using a 20 ppm spectral width, 16 K digitization points, a recycling delay of 1.5 s, 90° pulses of 5 μs and a composite pulse proton decoupling.

2.3.2. Solid state NMR

^{31}P and ^{2}H NMR experiments in MLV were performed at 162 and 61 MHz, respectively. Phosphorus spectra were recorded using a dipolar echo sequence ($\pi/2$–t–π–t) (Dennis and Plückthun, 1984) with a t value of 12 μs, a $-\pi/2$ pulse of 5 μs and a broadband proton decoupling. Phosphoric acid (85%) was used as external reference. Deuterium spectra were recorded by using a quadrupolar echo sequence ($\pi/2$–t–$\pi/2$–t) with a $\pi/2$ pulse of 8 μs, and a t value of 35 μs to form the echo. The free induction decay was shifted by fractions of the dwelling time to ensure that its effective time for the Fourier transform corresponds to the top of the echo (Dufourc et al., 1992). The sample temperature was regulated within 1 °C by a BVT-1000 unit.

^{2}H NMR spectra treatment: in order to extract suitable quadrupolar splitting measurements ($\Delta\nu Q$), the spectra were de-Paked according to Seelig (1977) procedure.

2.4. ESR experiments

Effect of CNTs on MLV fluidity was assessed by ESR spin label experiments. Two spin labels (Sigma France) were used: 5-nitroxide stearate (5 NS) and 16-nitroxide stearate (16 NS). These fatty acids self-incorporate the MLV and the nitroxide groups provide information of motional freedom of the label in the system. So the former probes the superficial part of the membrane layer, the latter in its hydrophobic core (Debouzy et al., 2007).

The experiments were performed on MLV made with DMPC 50 mg/ml. 0.8 mg of nanotube was added in 200 μl MLV solution and then labelled with 10 μl of spin label solution (5 ns 5×10^{-3} M or 16 ns 10^{-3} M). After 30 min incubation at room temperature, sample was transferred by capillarity in 20 μl Pyrex capillary tube. This tube was placed in a 3 mm diameter quartz holder, and insert into the cavity of the ESR spectrometer.

The ESR spectra were recorded at different controlled temperature (294, 295, 296, 297, 298 and 299 K) with the following conditions: microwave power 10.00 mW, modulation frequency 100 kHz, modulation amplitude 2.05 G, receiver gain 6.3×10^5 conversion time 81.92 ms, time constant 81.92 ms. Sweep range was 100 G with a central field value of 3435 G for 5 ns probe, and in the same condition except, modulation amplitude 1.03 G, receiver gain 10^5 conversion time 40.96 ms, time constant 81.92 ms for 16 ns probe.

The complete membrane incorporation of the spin labels was ascertained by the absence on the spectra of the extremely resolved ESR lines corresponding to free rotating markers.

5 NS experimentations: the values of outer and inner hyperfine splitting were measured ($2T_{\|}$ and $2T_{\perp}$, respectively), on ESR spectra (Fig. 4B), and order parameter S was calculated following the equation (Gaffney, 1976):

$$S = 1.723 \times \frac{T_{\|} - (T_{\perp} + C)}{T_{\|} + 2(T_{\perp} + C)} \quad \text{With } C = 1.4 - 0.053 \times (T_{\|} - T_{\perp})$$

The increase in the order parameter value means a decrease of local membrane fluidity.16 NS experimentations: the changes in freedom motion of 16 NS were analysed with the calculation of τ_c, the rotational correlation time. τ_c was calculated following the formula (Gornicki and Gutsze, 2000):

$$\tau_c = K \times \Delta W_0 \left(\sqrt{\frac{h_0}{h_{-1}}} - 1 \right) \quad \text{With } K = 6.5 \times 10^{-10}\,\text{s}\,\text{G}^{-1}$$

In this formula, ΔW_0 is the peak-to-peak line width of the central line; h_0 and h_{-1} are the peak height of the central and high-field lines, respectively (Fig. 4D).

The increase in the rotational correlation time means a decrease of local membrane fluidity.

3. Results and discussion

3.1. Detection of CNTs–phospholipid interactions

Previous results had evidenced the formation of suspensions formations of CNTs with lipids or surfactants (Moore et al., 2003). By considering that the cell matrix consists of important amounts of phospholipids – that bear two side chains of lipids – it was of interest to investigate possible interactions with pure phospholipids. As natural phospholipids are generally not soluble in water and self-organize in bilayers (Vance and Vance, 2008), we first tested a short-chained (C8) synthetic phospholipid, dioctanoyl-phosphatidyl choline that forms unilayer micelles and exhibits amphiphilic properties like some surfactants. In the presence of CNTs, no modifications of DOPC ^{1}H NMR spectra was observed (not shown) and we decided to use sonicated small unilamellar vesicles of egg lecithin, that also gives relatively resolved lines in ^{1}H NMR: this attempt also failed to evidence any interaction with CNTs, even if CNTs (0.5 mg) was added to SUV (7 mM) and vortexed, or co-sonicated with the lecithin. The absence of interaction with short-chained phospholipids was consistent with the overall hydrophobic properties of CNTs by opposition with the relatively amphiphilic properties of DOG. By contrast, SUV consist of long unsaturated phospholipids self-organized in rigid bilayers due to

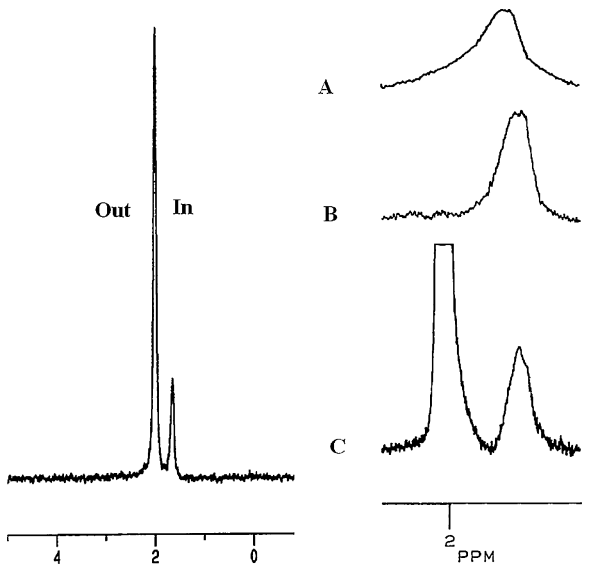

Fig. 1. ^{31}P NMR of LUV. Left: spectrum of LUV (EPC/EPA 9/1 M/M, 20 mM in NaH_2PO_4 0.4 M); extravesicular (out) and internal (in) contributions are separated by using a 1 u pH gradient. Right: (C) same as left spectrum with magnification for a better identification of intravesicular contribution; (B) same sample after addition of paramagnetic ions that broaden under detection the extravesicular contribution; (A) same sample in the presence of 1 mg CNTs after 3 h evolution.

the membrane curvature (radius about 10–20 nm), and the cohesion forces could be strong enough to preclude strong interactions with the relatively big size CNT systems.

This led to use other models of higher size, large unilamellar vesicles, LUV (EPC/phosphatidic acid 9/1 M/M, 20 mM), to observe membrane ionic permeability in the conditions of cation/proton exchange conditions, as classically described by Gary-Bobo and coworkers (Cybulska et al., 1986). Briefly, these membranes enclose a significant aqueous volume (20% of the total sample volume), thus separating two compartments, intra- and extravesicular. If the aqueous medium consists of NaH_2PO_4, ^{31}P NMR is a suitable tool to separate and identify on a spectrum the internal and external contributions by simply creating a pH gradient: hence, ^{31}P chemical shift directly depends on the pH, as classically described (Gorenstein, 1984). The result is shown on the insert of Fig. 1, and, plotted truncated on the bottom trace. Under these circumstances, pH equilibration induces a progressive shift of the internal resonance (high-field resonance) to the chemical shift corresponding to the external pH (the most intense peak). By adding 8 μl $MnCl_2$ 0.1 M, the resonance arising from the extravesicular contribution vanishes by paramagnetic effect, while the resonance of enclosed (not accessible to paramagnetic ion) phosphate remains unaffected (middle trace of Fig. 1). A slight line width broadening was simply observed (from 30 to 35 Hz), as a result of the paramagnetic effect on external deuterated water thus resulting in a loss of homogeneity. Successive spectra were then acquired up to 3 h (top trace). As no significant shift of the resonance occurred, it could be deduced that no membrane permeabilization had occurred (i.e. no ionophoric property). Furthermore, total signal intensity (the integral of the peak) was unchanged, indicating that no destruction of the LUV had occurred. However, a significant line broadening (to more than 55 Hz) strongly suggested that CNT–membrane interaction, at least a binding of CNTs at the surface had occurred: in the absence of any chemical shift variation, the line broadening could only be attributed to increased correlation time.

In order to study the dynamics and structural consequences of CNT presence, multibilayers of DMPC (dimyristoyl phosphatidyl choline) were finally used: MLV are big sized (up to 100 μm) multibilayers with very small intermembrane medium and relatively weak intramembrane cohesion forces. Such systems are well adapted to study dynamic and structural modifications, and the use of these systems and ^{31}P and ^{2}H solid state NMR, and ESR allowed to observe such parameters at the different levels of the membrane and to study of collective motions in the presence of highly concentrated models (80 mM) (Dufourc et al., 1992; Seelig, 1977).

3.2. ^{31}P NMR of DMPC dispersions (MLV)

The left trace presented on Fig. 2 is representative of axially symmetric powder phosphorus spectrum of standard bilayer structures of DMPC below phase transition (Debouzy et al., 1989). The temperature dependence of ^{31}P Chemical Shift Anisotropy (CSA, figured by an horizontal bar) was measured on the phosphorus-NMR spectra of multilayers (MLV) (Peinnequin et al., 2000) of pure DMPC or in the presence of CNTs (see legend of Fig. 2). As classically described (Duchene et al., 1992), CSA value can be considered as representative of the fluidity of the superficial part of a membrane, where phosphorus nuclei are located. By comparison with DMPC, no significant modification of the line shape was detected on the spectra of MLV in the presence of CNTs (under the same experimental conditions) indicating that the main bilayer structure was not significantly modified. Hence, no resolved resonance indicative of detergent effect or membrane destruction was observed at the isotropic position. Also, below 292 K, both line shape and the CSA values of pure DMPC and of CNT–DMPC systems were quite similar. By the way of contrast, a significant reduction of the CSA measured in the presence of CNTs occurred in the temperature domain, 294–298 K (295 K, see Fig. 2, right the top trace of

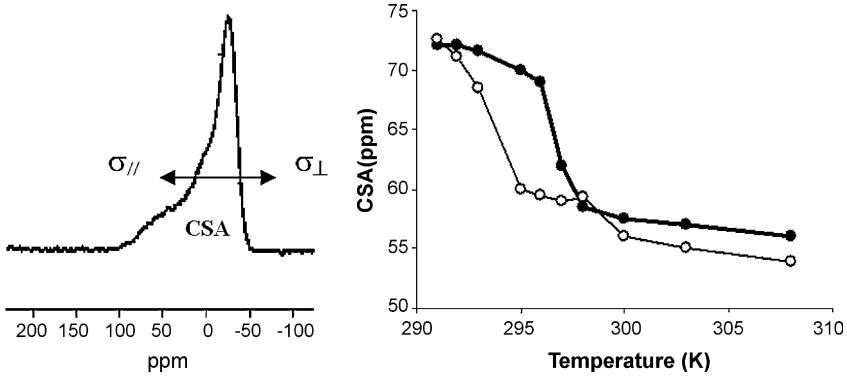

Fig. 2. ^{31}P NMR (left trace) of DMPC dispersion over transition temperature. The arrow represents CSA range (ppm), measured between the left shoulder ($\sigma_{//}$) and the high-field edge ($\sigma_{\perp}$) of the spectrum. Right: temperature dependence of the CSA, measured on pure DMPC (●), or on CNT–DMPC systems (1/50 W/W) (○).

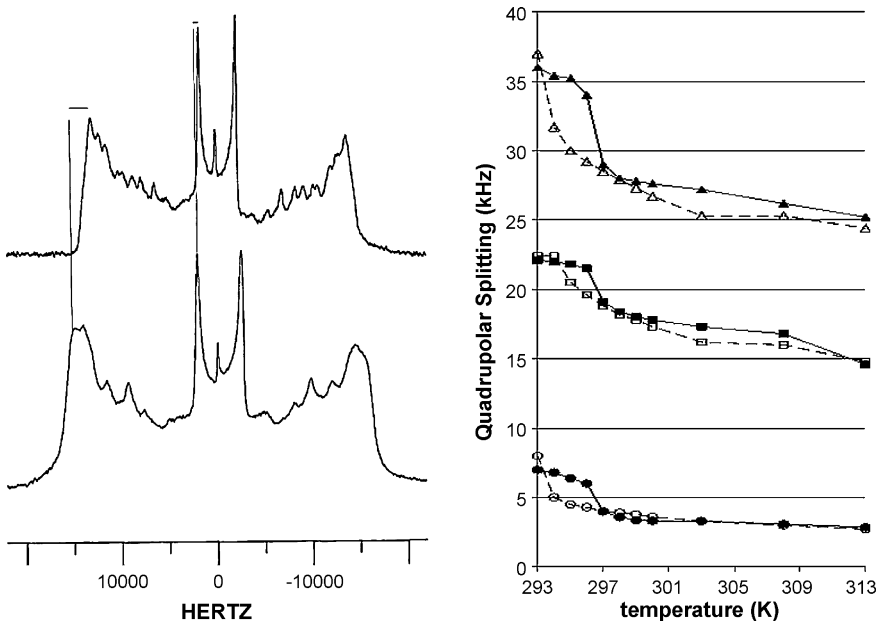

Fig. 3. ^{2}H NMR. Left bottom trace: spectra of DMPC-d_{54} below transition temperature (296 K) and (top trace) in the presence of CNTs (1/50 W/W). Quadrupolar splitting reductions are labelled with bars for the plateau region (outer doublet) and the terminal methyl group (inner doublet). Right: temperature dependence of quadrupolar splittings measured on the same samples, DMPC: on plateau region (▲), C10 doublet (■) and methyl doublet (●), and DMPC–CNTs system plateau region (△), C10 doublet (□) and methyl doublet (○).

CNTs/lipid 1/50 W/W). Besides, the phase transition temperature was found to be 2 K lower than that of pure DMPC, whereas the measures performed on traces at higher temperatures (298–313 K) also exhibited a significant reduction, revealing a higher fluidity at the polar head level where phosphorus is located.

3.3. ^{2}H NMR of chain perdeuterated DMPC liposomes

3.3.1. ^{2}H NMR lineshape

The bottom spectrum of DMPC-d_{54} dispersions (DMPC with perdeuterated chain) presented on the spectrum of Fig. 3 is typical of phospholipid bilayers below phase transition (temperature of 296 K) (Douliez et al., 1996; Fauvelle et al., 1997). Such a spectrum appears as a superimposition of symmetrical doublets, each doublet corresponding to a methylenic CD_2 group or to the terminal methyle CD_3 group of the acyl chain. For a given doublet, the splitting (quadrupolar splitting, $\Delta\nu Q$) is directly related to the local order following the relation:

$$\Delta\nu Q = \frac{A \times (3 \times \cos^2\theta - 1)}{2}$$

where A 170 kHz (for CD_2 bound in DMPC) and θ is the averaged value of the solid angle of reorientation. This splitting can be used in a first approximation as an order parameter. As the acyl chain fluidity decreases from the terminal methyl group (CD_3) to the methylenic groups close to the polar head of the lipids (the so called "plateau region", from C2 to C8 of the chain), the resulting spectrum consists of (i) an inner doublet with a quadrupolar splitting (in the 2–4 kHz range depending on temperature) attributed to the CD_3 methyl group, (ii) doublets with increasing quadrupolar splittings assigned to successive CD_2 groups from C14 to C9, (iii) the external edge doublet, attributed to the deuterium of the C2–C8 plateau region where quadrupolar splitting is measured between 24 and 30 kHz.

The spectra recorded in the same conditions in the presence CNTs (R = 1/50 W/W) exhibited significantly reduced values of quadrupolar splitting on all the doublets resonances (see CD_3, C10 and plateau curves on Fig. 3, left) in the low temperature range 293–298 K, indicating increased mobility of these groups of the layer. Besides, the traces are consistent with a 2 K lowering of the transition phase, whereas the part of the traces plotted at high temperature (i.e. over normal phase transition temperature for DMPC, 297 K) are quite similar to those of pure DMPC systems except for the plateau region, i.e. the most superficial groups of the chains. This feature is also supported by the corresponding lineshapes and linewidths: as shown on Fig. 3 (left), pure DMPC trace is typical of multilayers in gel phase below transition, 296 K (linewidth around 750 Hz for the CD_3 group) while reduced linewidths (linewidth of 600 Hz for CD_3 resonance) and splittings on CNTs containing systems reveal the presence of liquid crystal phase over transition temperature. It is also clear from the plots Fig. 3 (right), that the mobility of the different groups were inequally influenced by the presence of CNS at high temperature. While this fluidization is markedly observed for the superficial groups (the plateau region), this dynamic effect is less important in the middle of the chain (that vanishes at 313 K), and completely absent at the terminal methyl group level.

3.4. ESR experiments

ESR Spin label experiments were performed to assess the membrane fluidity in different temperature conditions. Two probes were separately used, 5 NS give information about superficial membrane fluidity, while 16 NS concerned the inner membrane region.

The overall result (Fig. 4) shows an increase in the mobility of the two probes contribution in the two groups with the temperature increase. As previously described in MLV model (Dufourc et al., 1992; Follot et al., 2009), the phase transition in control groups occurs near 297 K. The 5 NS results are drawn in Fig. 4A. A shift of the phase transition, 3° lower, could be observed in the nanotube group. In the inner compartment, 16 NS results (Fig. 4C) show a major effect of the carbon nanotubes with a total disappearance of phase transition, while it occurs at the same temperature as 5 NS experiments in the control group.

Thus, from all the results observed in multibilayer systems, it is apparent that a dramatic fluidization of the membrane is observed

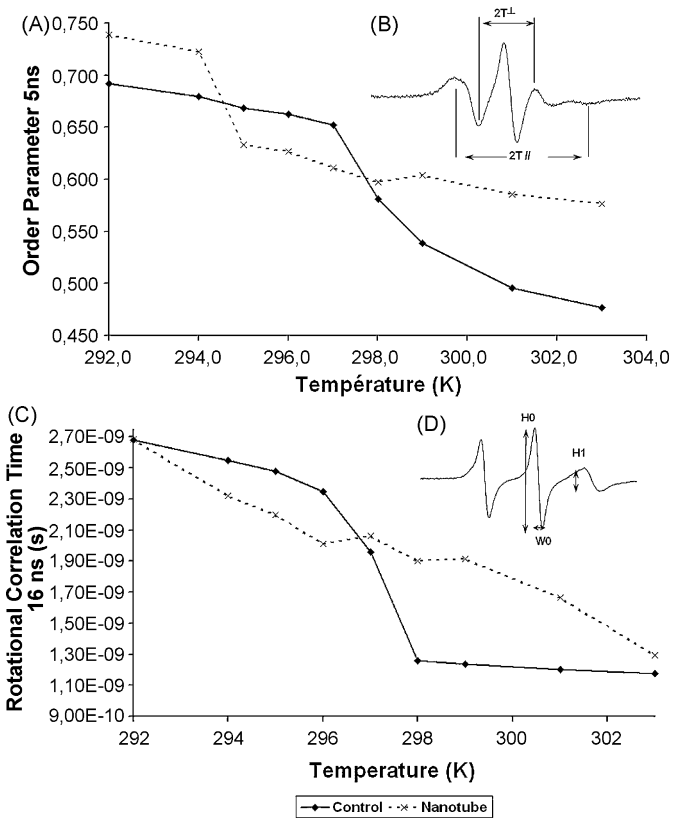

Fig. 4. ESR spin labeling experiment: (A) temperature dependence of the order parameter (5 NS) for pure DMPC (black diamond full line) and in the presence of DWNTs (black cross, dashed line); (B) typical 5 NS spectrum parameter used for order parameter estimation are inner ($2T_{\perp}$) and outer hyperfine ($2T_{||}$) splitting; (C) temperature dependence of the rotational correlation time (16 NS) for pure DMPC and in the presence of DWNTs; (D) typical 16 NS spectrum, parameter used for rotational correlation time was central peak intensity h_0, high-field peak intensity and the with of the mid-field line W_0.

below normal transition temperature (297 K for DMPC), and a 2 K lowering of this transition temperature. ^{31}P NMR CSA measurements also showed increased fluidity of the membrane at higher temperature at the surface, where phosphorus nuclei are located. This last point is significantly less markedly observed at the chain level, to be completely absent for the CD_3 groups, where only a lowering and smoothing of the Quadrupolar Splitting was noted. ESR experiments gave similar results for measurements performed at the terminal carbon of the spin labelled chain (doxyl stearate), whereas the shift of the transition temperature was less markedly observed, and a sole fluidizing effects found for more superficial labelling (5 NS). Steric hindrance of the label can result in a competition with CNTs themselves by opposition with NMR label that are true phospholipids identical as those of the membranes.

4. Conclusions

Regarding the possible biomedical uses of CNTs, for instance as drug carriers, their interactions with the membranes of living systems are a crucial feature. The DWNTs investigated in this study exhibit low cell toxicity in standard cell assays (neutral red or tetrazolinium tests) (Flahaut et al., 2006). Additionally, interactions have been reported with DNA (Lee and Mijovic, 2009), proteins (Salvador-Morales et al., 2006), and surfactants (Vance and Vance, 2008). Inflammatory induction or endocytosis has been extensively studied while the ability of functionalized CNTs to cross-membranes has been evoked (Pantarotto et al., 2004). This led us to investigate membrane–CNT interactions, and more precisely to observe the contribution of the phospholipid matrix and structure in such interactions. The present study shows that CNTs truly interact with model membranes, by inducing an overall fluidization of the layer more markedly observed at the superficial level, accompanied by a significant lowering of the transition temperature of DMPC dispersions. Besides, no significant modification of the main bilayer structure is present and no detergent effect of ionophoric property is found. The biological relevance of these results is the next step to investigate, using natural models (ghosts or erythrocytes) of living cells grown in labelled media to allow ^{2}H NMR studies, and finally to use a metabolomic approach of cell metabolism in the presence of CNTs, by HRMAS NMR methods. These investigations are now in progress.

Conflict of interest

The authors declare that there are no conflicts of interest.

References

Artyukhin, A.B., Shestakov, A., Harper, J., Bakajin, O., Stroeve, P., Noy, A., 2005. Functional one-dimensional lipid bilayers on carbon nanotube templates. J. Am. Chem. Soc. 127, 7538–7542.

Bronikowski, M.J., Willis, P.A., Colbert, D.T., Smith, K.A., Smalley, R.E., 2001. Gas-phase Production of Carbon Single-walled Nanotubes from Carbon Monoxide via the Hipco Process: A Parametric Study, 4th edition. AVS, Boston, MA, USA, pp. 1800–1805.

Cassell, A.M., Raymakers, J.A., Kong, J., Dai, H., 1999. Large scale CVD synthesis of single-walled carbon nanotubes. J. Phys. Chem. B 103, 6484–6492.

Cui, D., Tian, F., Ozkan, C.S., Wang, M., Gao, H., 2005. Effect of single wall carbon nanotubes on human HEK293 cells. Toxicol. Lett. 155, 73–85.

Cybulska, B., Herve, M., Borowski, E., Gary-Bobo, C.M., 1986. Effect of the polar head structure of polyene macrolide antifungal antibiotics on the mode of permeabilization of ergosterol- and cholesterol-containing lipidic vesicles studied by 31P-NMR. Mol. Pharmacol. 29, 293–298.

Debouzy, J.C., Crouzier, D., Gadelle, A., 2007. Physico chemical properties and membranes interactions of Per (6-desoxy-6-halogenated) cyclodextrins. Annales Pharmacologiques Francaises 65, 331–341.

Debouzy, J.C., Neumann, J.M., Herve, M., Daveloose, D., Viret, J., Apitz-Castro, R., 1989. Interaction of antiaggregant molecule ajoene with membranes. An ESR and 1H, 2H, 31P-NMR study. Eur. Biophys. J. 17, 211–216.

Dennis, E., Plückthun, A., 1984. Phosphorus 31P-NMR: Principles and Applications. Academic Press, London.

Donaldson, K., Aitken, R., Tran, L., Stone, V., Duffin, R., Forrest, G., Alexander, A., 2006. Carbon nanotubes: a review of their properties in relation to pulmonary toxicology and workplace safety. Toxicol. Sci. 92, 5–22.

Douliez, J.P., Léonard, A., Dufourc, E.J., 1996. H-NMR and neutron diffraction. J. Phys. Chem. 70, 18450–18457.

Duchene, P., Papalexiou, P., Ramis, J., Izquierdo, I., Houin, G., 1992. Pharmacokinetic profile of [14C]flutrimazole following single topical application in normal and scarified skin of healthy volunteers. Arzneimittelforschung 42, 861–863.

Dufourc, E.J., Mayer, C., Stohrer, J., Althoff, G., Kothe, G., 1992. Dynamics of phosphate head groups in biomembranes. Comprehensive analysis using phosphorus-31 nuclear magnetic resonance lineshape and relaxation time measurements. Biophys. J. 61, 42–57.

Englert, N., 2004. Fine particles and human health—a review of epidemiological studies. Toxicol. Lett. 149, 235–242.

Faraj, A.A., Lacroix, G., Alsaid, H., Elgrabi, D., Stupar, V., Robidel, F., Gaillard, S., Canet-Soulas, E., Crémillieux, Y., 2008. He and proton imaging of magnetite biodistribution in a rat model of instilled nanoparticles. Magn. Reson. Med. 59, 1298–1303.

Fauvelle, F., Debouzy, J.C., Crouzy, S., Göschl, M., Chapron, Y., 1997. Mechanism of &agr;-cyclodextrin-induced hemolysis. 1. The two-step extraction of phosphatidylinositol from the membrane. J. Pharm. Sci. 86, 935–943.

Flahaut, E., Bacsa, R., Peigney, A., Laurent, C., 2003. Gram-scale CCVD synthesis of double-walled carbon nanotubes. Chem. Commun. (Camb.), 1442–1443.

Flahaut, E., Durrieu, M.C., Remy-Zolghadri, M., Bareille, R., Baquey, C., 2006. Investigation of the cytotoxicity of CCVD carbon nanotubes towards human umbilical vein endothelial cells. Carbon 44, 1093–1099.

Follot, S., Debouzy, J.C., Crouzier, D., Enguehard-Gueiffier, C., Gueiffier, A., Nachon, F., Lefebvre, B., Fauvelle, F., 2009. Physicochemical properties and membrane interactions of anti-apoptotic derivatives 2-(4-fluorophenyl)-3-(pyridin-4-yl)imidazo[1,2-a]pyridine depending on the hydroxyalkylamino side chain length and conformation: an NMR and ESR study. Eur. J. Med. Chem. 44, 3509–3518.

Gaffney, B.J., 1976. Practical considerations for the calculation of order parameters for fatty acid or phospholipid spin labels in membranes. In: Berliner, R.J. (Ed.), Spin Labelling. Theory and Applications. Academic Press, New York, London, pp. 567–571.

Gorenstein, D., 1984. 31P-NMR: Principles and Applications. Academic press, London.
Gornicki, A., Gutsze, A., 2000. In vitro effects of ozone on human erythrocyte membranes: an EPR study. Acta Biochim. Pol. 47, 963–971.
Journet, C., Maser, W.K., Bernier, P., Loiseau, A., de la Chapelle, M.L., Lefrant, S., Deniard, P., Lee, R., Fischer, J.E., 1997. Large-scale production of single-walled carbon nanotubes by the electric-arc technique. Nature 388, 756–758.
Lee, H., Mijovic, J., 2009. Bio-nanocomplexes: DNA/surfactant/single-walled carbon nanotube interactions in electric field. Polymer 50, 881–890.
Lin, Y., Taylor, S., Li, H., Fernando, K.A.S., Qu, L., Wang, W., Gu, L., Zhou, B., Sun, Y.-P., 2004. Advances toward bioapplications of carbon nanotubes. J. Mater. Chem. 14, 527–541.
Mehra, N.K., Jain, A.K., Lodhi, N., Raj, R., Dubey, V., Mishra, D., Nahar, M., Jain, N.K., 2008. Challenges in the use of carbon nanotubes for biomedical applications. Crit. Rev. Ther. Drug Carrier Syst. 25, 169–206.
Monteiro-Riviere, N.A., Nemanich, R.J., Inman, A.O., Wang, Y.Y., Riviere, J.E., 2005. Multi-walled carbon nanotube interactions with human epidermal keratinocytes. Toxicol. Lett. 155, 377–384.
Moore, V.C., Strano, M.S., Haroz, E.H., Hauge, R.H., Smalley, R.E., Schmidt, J., Talmon, Y., 2003. Individually suspended single-walled carbon nanotubes in various surfactants. Nano Lett. 3, 1379–1382.
Ning, S., et al., 2007. Integrated molecular targeting of IGF1R and HER2 surface receptors and destruction of breast cancer cells using single wall carbon nanotubes. Nanotechnology 18, 315101.
Pantarotto, D., Briand, J.P., Prato, M., Bianco, A., 2004. Translocation of bioactive peptides across cell membranes by carbon nanotubes. Chem. Commun. (Camb.), 16–17.
Peinnequin, A., Piriou, A., Mathieu, J., Dabouis, V., Sebbah, C., Malabiau, R., Debouzy, J.C., 2000. Non-thermal effects of continuous 2.45 GHz microwaves on Fas-induced apoptosis in human Jurkat T-cell line. Bioelectrochemistry 51, 157–161.
Salvador-Morales, C., Flahaut, E., Sim, E., Sloan, J., Green, M.L., Sim, R.B., 2006. Complement activation and protein adsorption by carbon nanotubes. Mol. Immunol. 43, 193–201.
Seelig, J., 1977. Deuterium magnetic resonance: theory and application to lipid membranes. Quart. Rev. Biophys. 10, 353–418.
Stern, S.T., McNeil, S.E., 2008. Nanotechnology safety concerns revisited. Toxicol. Sci. 101, 4–21.
Thauvin, C., Rickling, S., Schultz, P., Celia, H., Meunier, S., Mioskowski, C., 2008. Carbon nanotubes as templates for polymerized lipid assemblies. Nat. Nanotechnol. 3, 743–748.
Thess, A., Lee, R., Nikolaev, P., Dai, H., Petit, P., Robert, J., Xu, C., Lee, Y.H., Kim, S.G., Rinzler, A.G., Colbert, D.T., Scuseria, G.E., Tomanek, D., Fischer, J.E., Smalley, R.E., 1996. Crystalline ropes of metallic carbon nanotubes. Science 273, 483–487.
Tian, F., Cui, D., Schwarz, H., Estrada, G.G., Kobayashi, H., 2006. Cytotoxicity of single-wall carbon nanotubes on human fibroblasts. Toxicol. In Vitro 20, 1202–1212.
Vance, D.E., Vance, J.E., 2008. Biochemistry of Lipids, Lipoproteins and Membranes, 5th edition. Elsevier, San Diego.
Wallace, E.J., Sansom, M.S.P., 2009. Carbon nanotube self-assembly with lipids and detergent: a molecular dynamics study. Nanotechnology 20, 045101.